Journal of the European Ceramic Society **18** (1998) 69–79

PII: S0955-2219(97)00100-3
0955-2219/98/$19.00 + 0.00

Fracture Energy Measurements of 2-D Carbon/Carbon Composites

V. Kostopoulos,[a]* Y. P. Markopoulos,[a] Y. Z. Pappas[a] and S. D. Peteves[b]

[a]Applied Mechanics Laboratory, University of Patras, University Campus, 265 00 Patras, Greece
[b]Institute for Advanced Materials, Joint Research Centre, European Commission, PO Box 2, 1755 ZG Petten, The Netherlands

(Received 17 March 1997; accepted 18 April 1997)

Abstract

*Fracture toughness of ceramic–matrix composites cannot be provided by an intrinsic fracture parameter. The presence of a fracture process zone induces stress redistribution mechanisms that partially shield the crack tip area from the applied stress field. The shape and size of the process zone depends upon extrinsic factors such as specimen shape and thickness, load distribution on the propagation zone, etc. The present work deals with the determination of the crack growth resistance curve (*R*-curve) of carbon/carbon (C/C) composites using the standard compact tension geometry. Two different material thicknesses were used and both monotonic and loading/unloading test patterns were applied. The determination of the* R*-curve in all cases was based on a compliance calibration technique. The results show that the monotonic loading leads to higher plateau values for the* R*-curve of the C/C material compared to that calculated from cyclic loading and referred to the same material thickness. Furthermore, the thicker specimens appear to have slightly higher plateau values. A precise examination of damage initiation and propagation was attempted to explain the monitored differences.* © *1997 Elsevier Science Limited.*

1 Introduction

Carbon/carbon composites are among the ideal candidate materials for high temperature structural applications due to their excellent specific mechanical performance up to 2500°C, good resistance to thermal shock and less brittle fracture behaviour compared to that of monolithic carbon.[1] Despite their sensitivity to oxidation, which could be overcome using oxidation protective top layer coatings,[2] C/C composites have no competitor in high temperature–high strength applications.

C/C composites can be considered as tough materials made of brittle constituents; high mechanical performance fibers are organized in a compliant preform and stabilized together with a poor mechanical performance carbon matrix.[3] This kind of structure, in the presence of a strain concentration site, permits the development of a damage process zone where stress redistribution occurs by extensive matrix cracking, fibre-matrix debonding and sliding, accompanied by stochastic fibre fracture[4,5] offering, in such a way, partial shielding of the crack tip region from the applied load.

According to recent literature,[6–8] C/C materials, in the presence of a structural discontinuity under mode I remote loading, display shear type damage, which provides the formation of shear bands normal to the initial notch plane.

Many attempts have been made at fracture behaviour characterization of C/C composites. It is generally accepted that the fracture behaviour of a ceramic–matrix and the C/C composites can be better illustrated by the crack growth resistance curve (*R*-curve) of the material, rather than through the determination of an intrinsic material parameter, which seems to be hopeless.[9–11] Due to the lack of testing standards in the case of ceramic–matrix composites, different specimen geometries and different theoretical approaches, assuming either linear or non-linear, elastic or non-elastic material behaviour, have been used in order to analyse the resistance to damage propagation of C/C composites. As a result, a large amount of experimental data have been produced, often conflicting.[12–15]

Within the scope of the present work, interest was centered on the compact tension (CT) test, which used for mode I fracture toughness characterization

*To whom correspondence should be addressed.

of C/C material normal to the plane of the reinforcements. It is the authors' opinion that the CT test offers the advantages of being less likely to promote compressive yielding compared to the bend specimen, and reserves a zone where stable crack propagation of the initial crack occurs.

The aim of the present work is (i) to compare the *R*-curve behaviour of C/C composites resulting under monotonic and cyclic loading, (ii) to investigate the effect of the thickness of the specimens on their fracture behaviour and (iii) to identify the fracture modes and the mechanisms which take place during the loading process.

To this end, in the case of monotonic tensile loading, the approach of effective crack length, which is provided via the compliance calibration procedure, was adopted, together with the assumption of the validity of linear elastic fracture mechanics (LEFM). In the case of cyclic loading the behaviour of C/C material was modeled as a sum of two contributions; a linear elastic one that fails according to the principles of LEFM, and an independent damage mechanism which absorbs energy but does not alter the ultimate fracture load. The energy absorbing mechanism is responsible for the irreversible deformation of the material.

In Section 2 complete descriptions of the material used and the experimental procedure followed are given, whilst in Sections 3 and 4 the analysis of the experiments conducted under monotonic, and cyclic, loading is presented respectively. Section 5 contains the results for the crack growth resistance curves of the materials under investigation, under both loading patterns together with a systematic comparison and discussion of the failure modes detected using SEM microscopy. Finally, Section 6 summarises some basic conclusive results and argues some aspects of the analytical modeling of the fracture behaviour of C/C composites based on the bridging stress approach.

2 Experimental Procedure

2.1 Description of the material

Commercially available 2-D carbon/carbon laminates produced by Schunk Kohlnenstofftechnik GmbH were tested. The laminates were reinforced by orthogonally woven 8-harness satin weave fabric, stacked together in a symmetric (0°/90°) way. The fabric contained high tensile modulus fibers and the base matrix material was phenolic resin. The production of the material consisted of a series of carbonisation (800°C) and re-impregnation with phenolic resin cycles plus a final graphitisation post-treatment cycle (2100°C). The final fiber volume fraction of the C/C plates was 60% and the total porosity of the material was less than 10%. The bulk density of the material was 1·49 g cm^{-3}. Two different plate thickness were tested, one of 2·7 mm and one of 10 mm.

The tensile properties of the material are given in Table 1 and they are identical both for plate thickness and in both plate directions, as expected.

The tensile tests were performed using dog-bone shape specimens, 210 mm long and 10 mm wide (at the ligament region). The cross head velocity of the hydraulic testing machine used for the tensile tests was 0·1 mm min^{-1}. The material exhibited a slight non-linear behaviour approaching the end of its life. A typical stress–strain curve is given in Fig. 1. The thickness of the tested specimen reported in Fig. 1 was 2·7 mm.

2.2 Testing procedure

As previously stated, two different plate thicknesses were tested under monotonic and cyclic loading, in order to obtain the *R*-curve behaviour of the 2-D C/C composites. In all cases the CT test was adopted and a schematic representation of test coupons, the dimensions of which are according to the European Structural and Integrity Society test protocol, is given in Fig. 2. The dimension *W* has been chosen to be 40 mm.

Mechanical loading was applied through a pin-and-shackle system to prevent the specimen from bending. The cross head velocity of the testing machine was 0·1 mm min^{-1}. The crack geometry was of V-shape. The notches were prepared using a diamond saw for the initial cut, a razor blade being

Table 1. Tensile properties of the 2-D woven C/C composite

Tensile strength (MPa)	173
Modulus of elasticity (GPa)	60
Poisson's ratio	0·07

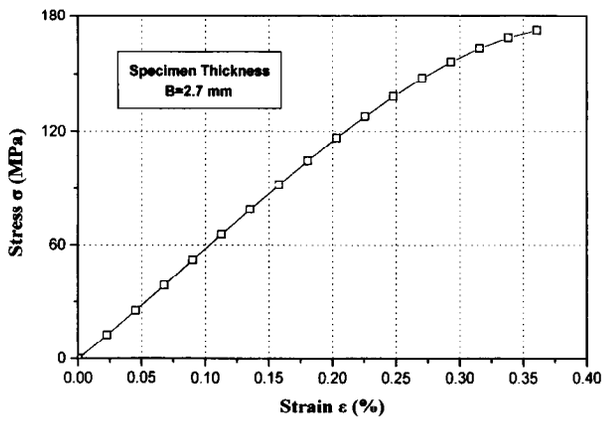

Fig. 1. Representative stress–strain curve of the 2D C/C material ($B = 2{\cdot}7$ mm).

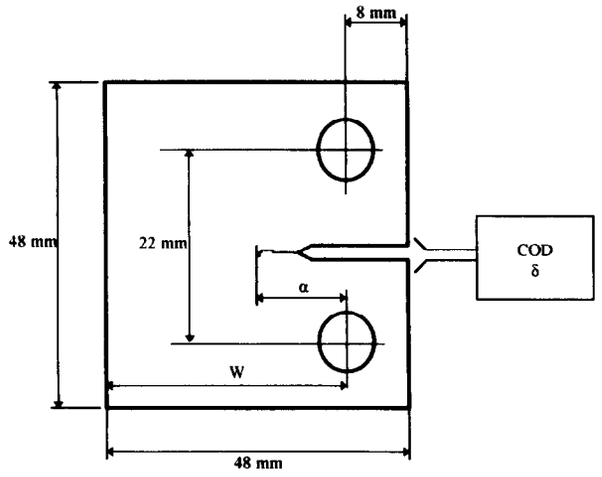

Fig. 2. Schematical representation of the compact tension test specimen.

used for the final cut at the crack tip. A special jig was applied to ensure that each razor cut was uniform and at the right angle with respect to specimen direction. The edge radius of the razor blade was 0·003 mm.

3 Monotonic Tensile Loading of the CT Specimen

Thin and thick specimens were used for the determination of the *R*-curve behaviour of 2-D C/C composites using LEFM analysis, adopting the compliance calibration technique. This approach is valid whenever small scale energy absorbing mechanisms are present.

This is mainly the case for thin specimens, where it was evident that the presence of limited residual displacements, after several loading/unloading cycles applied on a CT specimen, were attributed to a limited amount of low scale debris effect. Thus, the assumption of the absence of independent damage mechanisms validates the consideration of the test coupons as damageable linear elastic materials.

The experimental procedure consisted of the following steps:

3.1 Generation of the compliance calibration curve

It is well known that a macrocrack can be defined, in the case of ceramic composites, as a material region for which the level of damage is so extensive that its rigidity is negligible. Therefore, the development of a damage zone affects the specimen compliance in the same way as crack propagation. This approach justifies the use of a compliance calibration curve $C(\alpha)$, which correlates the propagation of the damage zone to the notch lengths of specimens, cut with a thin diamond saw (0·3 mm thickness) in order to retain the same compliance. The calibration curve allows the determination of an effective macrocrack length from the compliance measurements. In the present work, compliance calibration curves were determined using crack mouth opening measured by a crack opening displacement (COD) transducer.

3.2 Application of the LEFM approach

In both cases, of thin and thick 2-D C/C composites, the LEFM was applied for the calculation of the strain energy release rate according to the well known relation:

$$G_R = \frac{P_c^2}{2B}\frac{dC}{d\alpha} \tag{1}$$

where P_c is the fracture load at each crack increment, B the specimen thickness and $\frac{dC}{d\alpha}$ the slope of the compliance calibration curve at that point which is described by the calculated crack length. In addition the material fracture toughness K_{IC} is calculated using the following equation:

$$K_{IC}(\alpha) = \frac{P(\alpha)}{B\sqrt{W}} Y\left(\frac{\alpha}{W}\right) \tag{2}$$

where:

$$Y\left(\frac{\alpha}{W}\right) = \left(2+\left(\frac{\alpha}{W}\right)\right)\left(1-\left(\frac{\alpha}{W}\right)\right)^{-3/2} \left\{0{\cdot}886 + 4{\cdot}64\left(\frac{\alpha}{W}\right) - 13{\cdot}32\left(\frac{\alpha}{W}\right)^2 + 14{\cdot}72\left(\frac{\alpha}{W}\right)^3 - 5{\cdot}6\left(\frac{\alpha}{W}\right)^4\right\} \tag{3}$$

This expression is accurate within 0·5% in the range of $0{\cdot}2 < \alpha/W < 1$. Finally, within the bounds of LEFM, the existing relation between G_R and K_{IC} is given by the expression:

$$G_R = \frac{K_{IC}^2}{E'} \tag{4}$$

where $E' = E$ under plane stress and $E' = E/(1-\nu^2)$ under plane strain conditions.

3.3 Plot of the energy release rate against the effective crack length

The change of crack length during the monotonic loading was computed from the change in compliance. This method provides a safe way to obtain the elastic strain energy release rate assuming the material is a damageable elastic one. The *R*-curve is provided by plotting the strain energy release rate versus the apparent crack increment $\Delta\alpha$.

As already stated, this kind of approach to fracture behaviour of 2-D C/C material involves remarkable uncertainties mainly in the case of thick specimens, where the presence of 'irreversible damage mechanisms' affects the resulting R-curve, thus overestimating the fracture resistance of the material.

4 Cyclic Loading of CT Specimens

In order to reveal the irreversible damage mechanisms occurring in the vicinity of the crack tip during the monotonic loading, a loading/unloading procedure has been applied under displacement control of the testing frame.

The test specimen was unloaded to about 50% of each previous load so that the slope of the unloading line (e.g. the inverse of compliance) could be determined. The specimen was then reloaded. It was possible to repeat this loading/unloading pattern five to six times until the final fracture of the test coupon. The loading rate was again 0·1 mm min^{-1}.

Following the above described cyclic loading one could apply the technique proposed in Ref. 16 for the calculation of the J-integral which describes the energy release rate in the case of non-linear, elastic fracture mechanics approach. The present analysis, which was again applied on both thin and thick specimens, aims to determining the crack growth resistance R of the 2-D C/C material as the sum of two energy rate contributions:

- the non-linear strain energy release rate G_R^*, which can be directly correlated to G_{IC} fracture parameter, calculated by LEFM;
- the plastic energy dissipation rate Φ_{ir}, which is the energy consumed due to the process of the formation of the damage zone which surrounds the crack tip region.

The crack growth resistance R, the nonlinear strain energy release rate G_R^* and the plastic energy dissipation rate Φ_{ir} were calculated using the loading/unloading procedure applied for the CT specimen configuration. The establishment of this nonlinear semi-empirical approach, based on the form of the $(P - \delta)$ curve at each stage of crack increment, is a necessary requirement in order to understand the fracture behaviour of 2-D C/C composite materials, track down the inherent irreversible mechanisms and calculate the consumed energy rates needed for the formation of the crack area.

In Fig. 3, a representative curve of the linear elastic fracture behaviour is shown. At the instant a critical load is reached, a crack increment occurs.

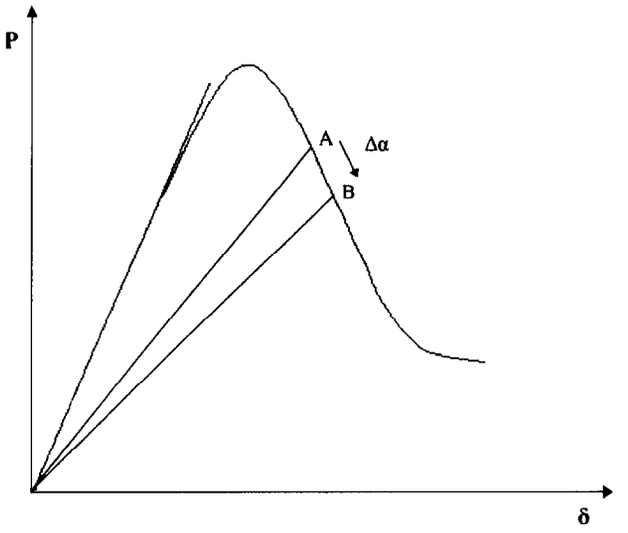

Fig. 3. Typical $(P - \delta)$ curve—linear elastic behaviour.

As a result the curve exhibits a non-linear form. Successive unloading, (Fig. 3), at different stages of crack propagation, shows that no plastic phenomena are present. In this case, the characteristic parameters are the load P, the crack opening displacement δ and the compliance from the origin, $C = \frac{\delta}{P}$. Therefore, the effective crack length may be easily calculated. Additionally, it is obvious that the non linearity of the $(P - \delta)$ curve is only attributable to the irreversible loss of energy consumed to create a new crack surface.

Figure 4 shows a schematic representation of the behaviour of a linear, non-elastic material. The crack propagates when a critical load is exceeded. In this case, successive unloading at different crack increments leads to plastic deformation as a result of the development of various additional fracture mechanisms such as fibre bridging and pull-out, fiber-matrix debonding, debris effects, and extensive matrix microcracking. The consumed total

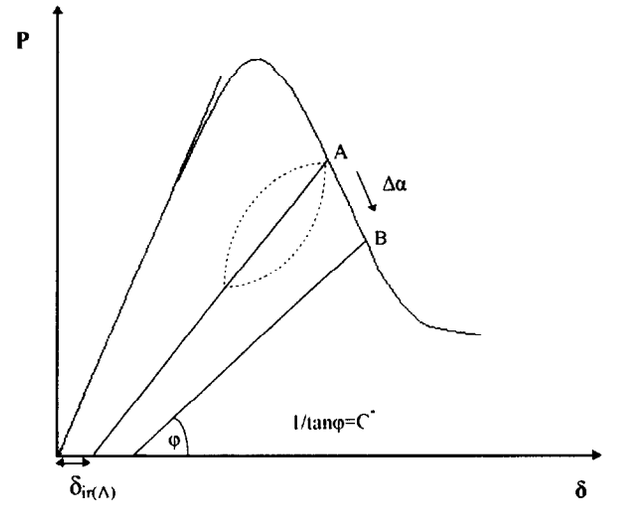

Fig. 4. Representative curve of linear non-elastic behaviour.

energy now consists of the part necessary for the formation of new crack surface and the energy, and that necessary for supplying all the 'irreversible' damage mechanisms which appeared.

The characteristic parameters are the load P, the COD δ, the remaining displacement at each unloading step δ_{ir} as well as the modified compliance C^*, $C^* = \frac{\delta - \delta_{ir}}{P}$.

When the loops of the loading cycles are not linear, a non-linear, non-elastic behaviour is assigned. Using the medians to the loops one may apply the same calculation procedure which is presented in the following. The main reason for using the loading/unloading procedure is that the irreversible mechanisms are traced via the registration of the residual displacements δ_{ir}. The variation of compliance C^* between two successive cycles, $n-1$ and n, permits estimation of the crack increment using an experimentally well established formula:[13, 17]

$$\alpha_n = \alpha_{n-1} + \frac{b_{n-1}}{2} \frac{C_n^* - C_{n-1}^*}{C_n^*} \tag{5}$$

where:

α_n, α_{n-1} = crack length at the two successive cycles n, $n-1$, respectively;

C_n^*, C_{n-1}^* = the corresponding modified compliance during the cycles n and $n-1$;

$b_n = W - \alpha_n$ = uncracked ligament of the specimen after n-cycles.

Thus at each unloading stage one may assign an effective crack length α_{eff}, as shown in Fig. 5. In general the total energy consumed for crack propagation from α to $\alpha + \Delta\alpha$ consists of two contributions:

- the energy to create a new crack surface ΔA, Γ;
- the energy dissipated to the irreversible mechanisms due to material structure, U_{ir}.

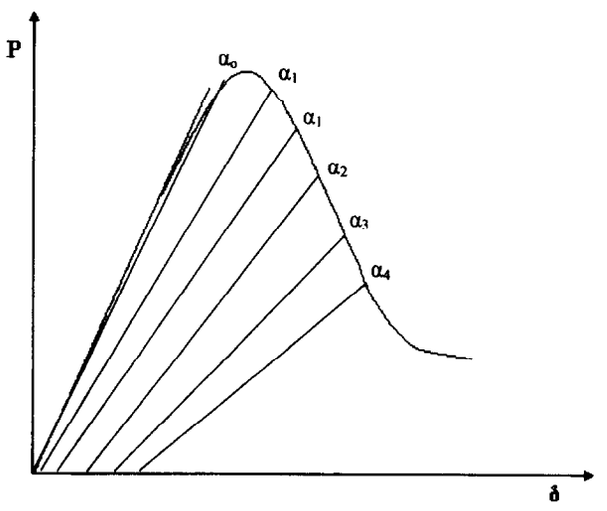

Fig. 5. Calculation of the effective crack length using the change of the modified compliance.

The energy contribution U_{ir} may highly exceed the necessary energy for the creation of the crack surface, Γ. Thus, its magnitude belongs among the important parameters which must be determined for the characterization of the fracture behaviour of a macroscopically non-elastic material. In Fig. 6, which is a $(P-\delta)$ curve of such a material, the definition of all the energy parameters involved in the procedure of fracture characterization are given. The assumption made is that the crack propagates in a slow and stable way due to the external energy supply and the kinetic energy of the system is negligible.

The total mechanical energy, W, given to the system for crack growth has the following form:

$$W = U_e + U_p + \Gamma \tag{6}$$

where:

W = the total work given to the system externally;

U_e = the elastic energy;

U_{ir} = the energy loss due to irreversible phenomena;

Γ = the energy for the formation of a new crack surface.

For a quasi-static increment of crack surface $\delta A = B\delta\alpha$, G_R^* is the elastic energy release rate, given by the rate of change of the area O'AE (Fig. 6). As a result G_R^*, is the rate of change of crack advance energy Γ. For the elastic deformation, the strain energy component is given by:

$$U_e = \frac{1}{2}P(\delta - \delta_{ir}) = \frac{1}{2}P^2\left(\frac{\delta - \delta_{ir}}{P}\right) = \frac{1}{2}P^2C^* \tag{7}$$

The elastic energy release rate is therefore:

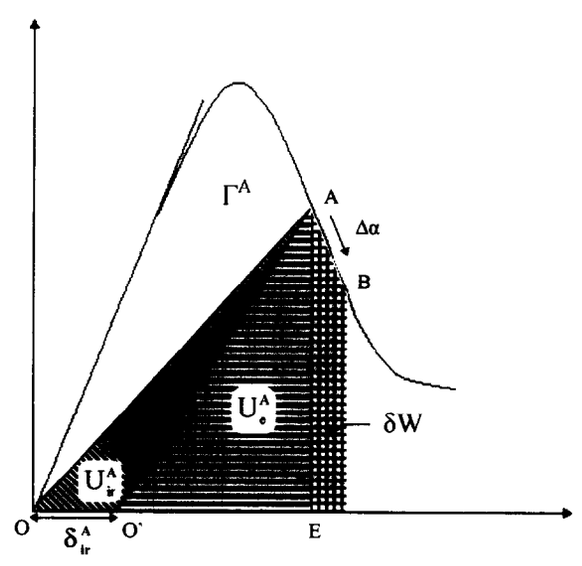

Fig. 6. Determination of the energy values in a $(P-\delta)$ curve for a linear non-elastic material behaviour.

$$\frac{dU_e}{d\alpha} = PC^* \frac{dP}{d\alpha} + \frac{P^2}{2}\frac{dC^*}{d\alpha} \tag{8}$$

According to Ref. 17 and Fig. 6, a fraction $\lambda(\%)$ of the total mechanical energy input W corresponds to the irreversible mechanisms energy U_{ir} at each crack growth stage, and it is given as the ratio of the areas, OAO′ (U_{ir}) and OAEO (W):

$$\lambda_i = \frac{U_{ir}}{W} \Big|_{\alpha_{effi}} \tag{9}$$

Differentiating eqn (4) and taking into account eqn (7) the modified potential energy release rate G_R^* is given by:

$$G_R^* = \frac{(1-\lambda)}{B}\frac{P d\delta}{d\alpha} - \frac{PC^*}{B}\frac{dP}{d\alpha} - \frac{P^2}{2B}\frac{dC^*}{d\alpha} \tag{10}$$

It should be noted that the component $\frac{dP}{d\alpha}$ cannot be neglected since irreversible mechanisms are presented, thus this quantity should be calculated for each loading/unloading cycle. Furthermore neglecting the quantity $\frac{dP}{d\alpha}$ and assuming that λ ratio tends to zero LEFM approach is obtained as a special case of eqn (10).

The energy rate Φ_{ir} coming from the non-elastic energy part, which is associated with the irreversible mechanisms due to development of the damage zone in the vicinity of the crack tip, is given by the relation:

$$\Phi_{ir} = \lambda \frac{P\, d\delta}{B\, d\alpha} \tag{11}$$

According to the previous analysis, the experimental evaluation of the energy release rate values G_R^* and Φ_{ir} is based on the following steps:

- Monitoring of the $(P-\delta)$ curve during loading/unloading cycles;
- Calculation of δ, δ_{ir}, P and C^* for each cycle;
- Evaluation of effective crack increment using Fig. 3 for the nth loading/unloading cycles;
- Determination of the functions $P(\alpha_{\text{eff}})$ and $\delta(\alpha_{\text{eff}})$;
- Numerical integration for the evaluation of the external work offering to the system, W, and the non-elastic energy U_{ir} for the calculation of energy ratio λ.

5 Results and Discussion

5.1 Monotonic loading—LEFM analysis

The compliance calibration curves for the thin and thick specimens are presented in Fig. 7(a) and (b),

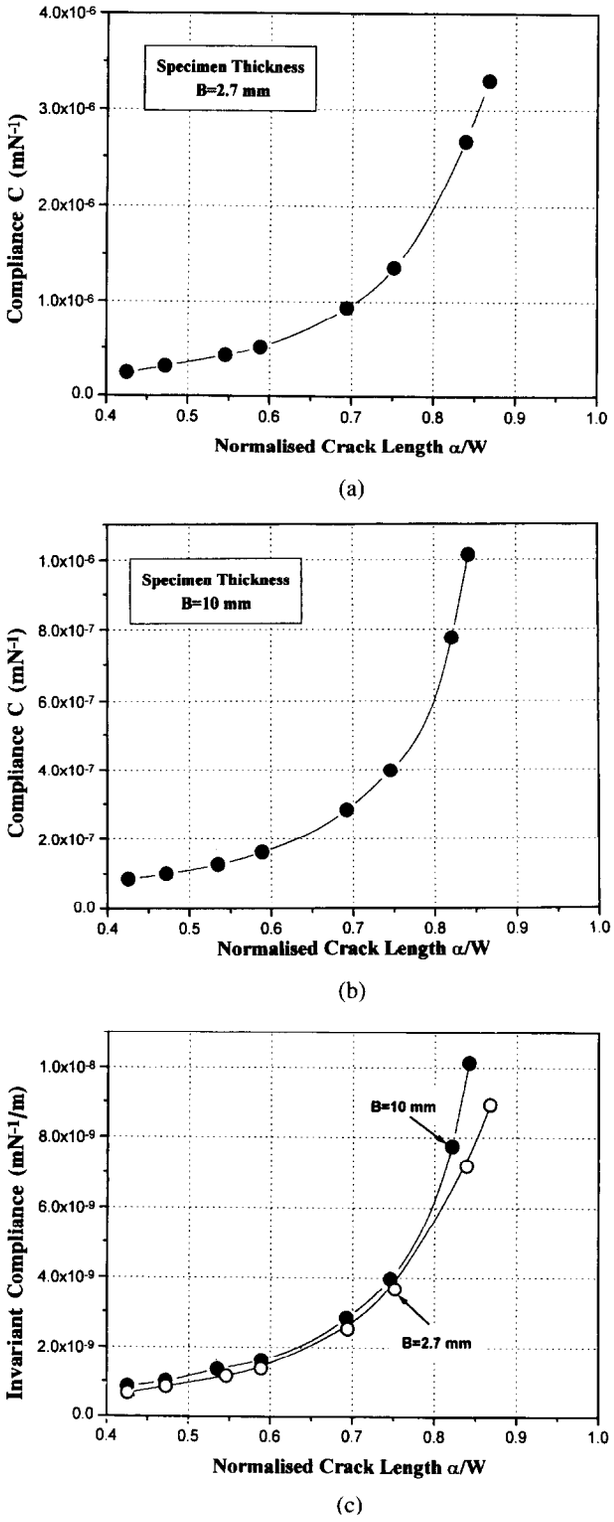

Fig. 7. Compliance calibration curves (a) $B=2{\cdot}7$; (b) $B=10$ mm and (c) invariant compliances.

respectively. Figure 7(c) illustrates the normalized compliance, with respect to the specimen thickness, for both thin and thick specimens. As shown, the two normalized compliance curves are very close as was expected, since the normalized compliance referred to the same specimen geometry and could be considered as a kind of material constant. Figure 8 presents a typical normalized load-displacement curve for both thin and thick specimens.

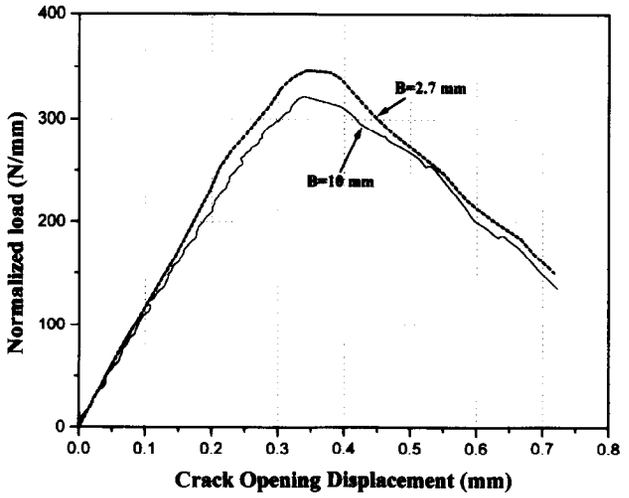

Fig. 8. Typical normalized load versus crack opening displacement for both specimen thicknesses.

It is obvious that the results are slightly affected by the specimen thickness. Although the maximum normalized load values (P/B) are about the same, in thick specimens the slight non-linear behaviour appeared earlier or, in other words, it appeared to be more compliant for loads over 60% of the fracture load.

The application of the compliance calibration procedure to calculation of the strain energy release rate G_{IC} leads to the results illustrated in Fig. 9 for thick and thin specimens. In both cases, an initial notch size of $\alpha_o = 17$ mm was used.

The plateau value of the strain energy release rate for the thick specimen is 8 kJ m^{-2}, which is slightly increased compared to the relative value given by the thin specimen which is close to 7 kJ m^{-2}. This difference is explained based on the following arguments. Since the thick specimen is more compliant for loads close to the failure load, this leads to higher effective crack length values. Conversely,

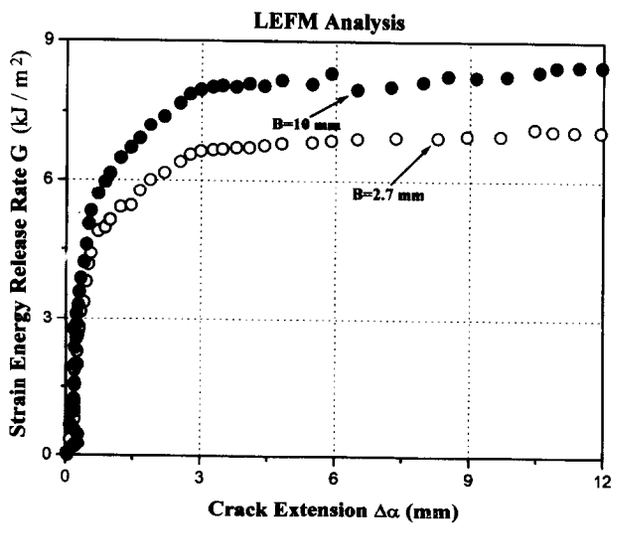

Fig. 9. Strain energy release rates, G_{IC} using linear elastic fracture mechanics.

taking into account that the slope of the compliance is an increase function of the effective crack length, as shown in Fig. 7, higher effective crack values lead to higher values of the derivative

$$\frac{\partial C}{\partial \alpha}\Big|_{\alpha_{\text{eff}}}$$

and as a result to higher plateau values of the strain energy release rate.

The monitored plateau region in both cases of thin and thick specimen is of the same size, about 11 mm long and after that a high increase rate of the energy release rate appears due to the compressive stress field which is developed due to the bending of the rear side of the CT specimen. The size of the plateau is in agreement with the calculations which have been made in Ref. 18 and show that the compressive field begins after a normalized length of $\bar{x} = (\frac{x}{(W-\alpha)}) = 0{\cdot}6$.

Assuming linear elastic behaviour for the 2D-C/C material and using eqn (2), the fracture toughness K_{IC} is obtained to be about 15 MPa$\sqrt{\text{m}}$ for both thin and thick specimens, which is very close to the value of the fracture toughness reported in Ref. 15 ($K_{IC} = 16$ MPa$\sqrt{\text{m}}$). However the assumption of the linear material behaviour gives rise to eqn (4), the application of which gives $K_{IC} = 25$ MPa$\sqrt{\text{m}}$ for the thick specimen and $K_{IC} = 20{\cdot}5$ MPa$\sqrt{\text{m}}$ for the thin one. Although the above described procedure for the characterization of the fracture behaviour of 2-D C/C material is remarkably easy to apply, the obtained results demonstrate all the uncertainties involved in the method.

5.2 Cyclic tests—NLEFM analysis

In this case, the material fracture behaviour is considered as a non-linear, non-elastic one. The crack growth resistance R is assumed to be the sum of the energy release rate for the crack advance, when the material under consideration responses in a non-linear elastic manner, (J-integral), and the plastic energy dissipated rate which is consumed for the formation of the irreversible phenomena and the damage process zone.

For the determination of non-linear fracture mechanics energy parameters, the cyclic ($P - \delta$) curves should be analyzed according to the semi-empirical procedure described in Section 4.

A typical loading–unloading ($P - \delta$) curve is presented in Fig. 10 for the thick specimens. Then a detailed analysis is conducted in order to calculate the load P, the crack opening displacement δ, the irreversible remaining displacement δ_{ir} at each unloading stage and the modified compliance C^*. Based on that, the effective crack length, α_{eff}, at the

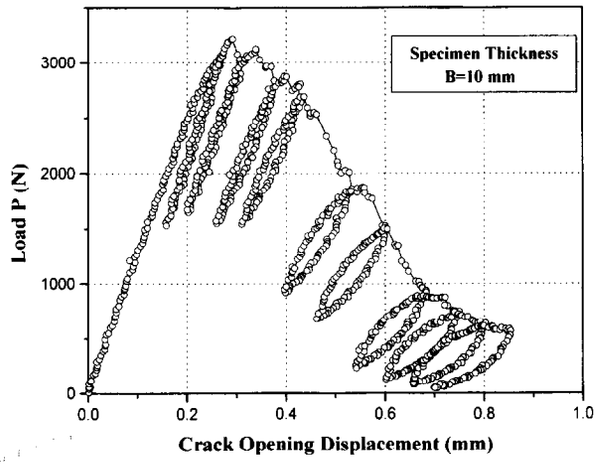

Fig. 10. Typical loading–unloading curve for a thick specimen ($B = 10$ mm).

nth loading–unloading cycle is evaluated using the recurrence relation of eqn (5). Furthermore, based on $(P - \delta)$ curve, the plastic dissipated energy ratio λ can be easily defined according to eqn (9). The obtained results from the above described analysis are given in Fig. 11(a)–(d). In all the cases, data have been kept only up to a normalized distance

$$\bar{x} = (x/(W - \alpha)) = 0{\cdot}6$$

After that the compressive field starts to act and the data are misleading.

It is quite interesting to focus for a while on the $\lambda(\alpha_{\text{eff}})$ curve illustrated in Fig. 11(c). It is evident that in the early stages of crack propagation the ratio of irreversible plastic energy dissipated to the total mechanical energy input is very small, namely 10–15%, and this becomes clear from the form of $(P - \delta)$ curve together with the small value of the irreversible displacements δ_{ir} for each loading–unloading loop. For the thin specimens the ratio of dissipated energy λ is lower, of the order of 6–10%. When stable crack propagation initiates, the ratio λ rapidly increases and reaches a plateau value. This is due to the complete development of the fracture process zone which mainly consists of a cracked matrix, bridged by intact and/or failed fibers, which debond, slip and pull out. Crack bridging enhances material crack resistance by partially shielding the crack tip from the applied load. Further crack advance over a critical length leads to the interaction of the fracture process zone with the compressive field generated from the

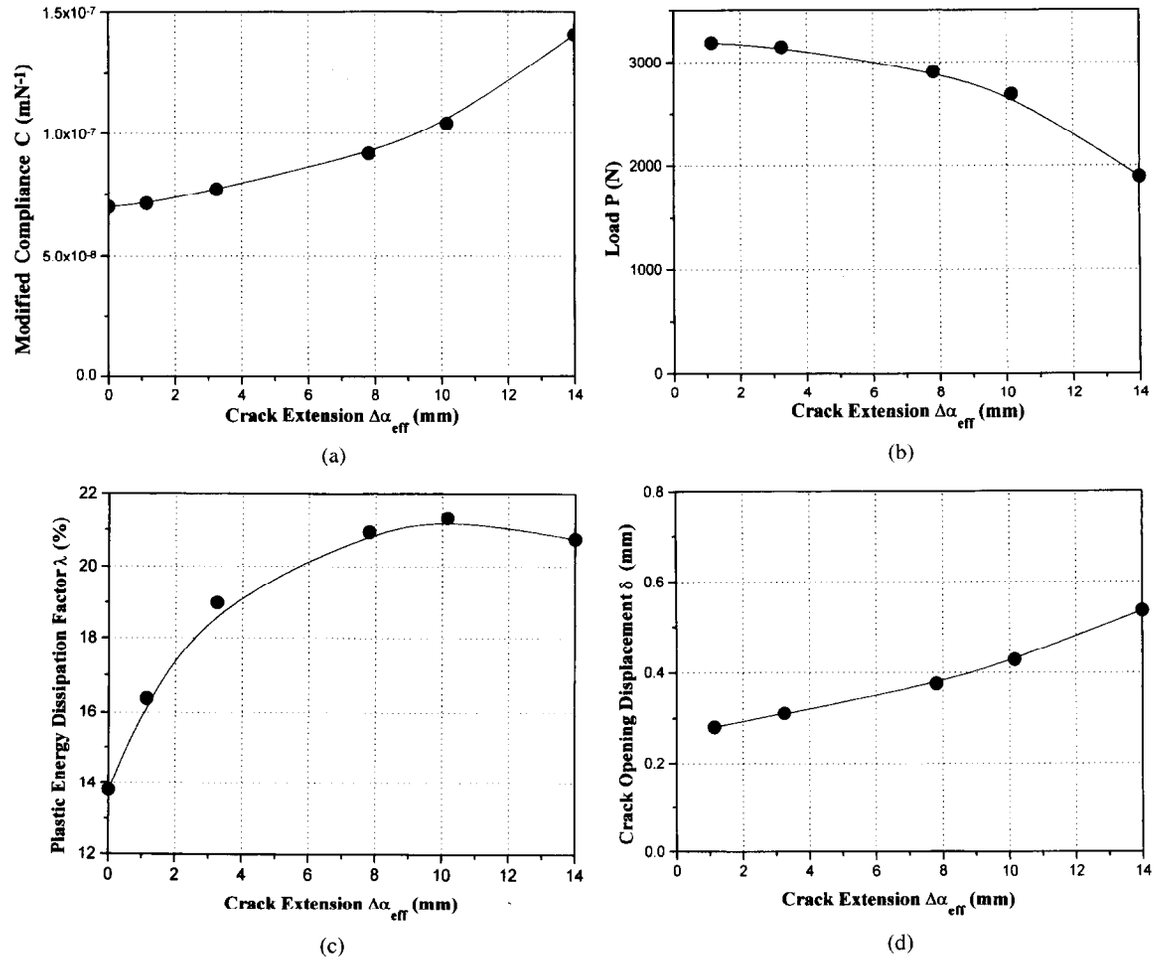

Fig. 11. Parameters of the proposed analysis described in Section 4. (a) Modified compliance versus effective crack extension; (b) load versus effective crack extension; (c) energy dissipation rate λ versus effective crack extension; (d) crack opening displacement versus effective crack extension.

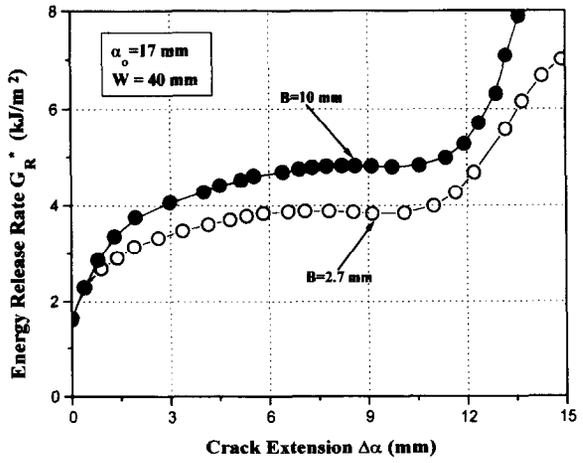

Fig. 12. Elastic energy release rate, G_R^*, versus effective crack extension, $\Delta\alpha_{\text{eff}}$, for thin ($B = 2{\cdot}7$ mm) and thick ($B = 10$ mm) specimens.

bending of the rear surface of the CT sample. This interaction becomes dominant and a fast increase of the λ ratio appears. Figure 12 shows the elastic energy release rate G_R^*, for both thin and thick specimens versus the effective crack extension $\Delta\alpha_{\text{eff}}$.

Initially the energy increases as the crack propagates, for $\Delta\alpha_{eff} \sim 2{\cdot}5$ mm. This value is nearly the same for both thick and thin specimens. Then, the energy remains almost constant appearing slightly different between the plateau values which correspond to the thin and thick specimens. This plateau value is, for the thin one, $G_R^{*\text{thin}} = 3$–$3{\cdot}5\,\text{kJ m}^{-2}$, and for the thick one $G_R^{*\text{thick}} = 3{\cdot}5$–$4{\cdot}5\,\text{kJ m}^{-2}$. The length of the plateau region is about 10 mm and appears to be common to both cases.

The associated stress intensity factor (SIF) (if one could permit this kind of interpretation to the definition of SIF) is $K_R \approx 16\ \text{MPa}\sqrt{\text{m}}$. This is in agreement with the value of SIF calculated earlier during the analysis of the monotonic tensile loading experiments when the LEFM was applied. This is also the value of the SIF reported in Ref. 15.

In Fig. 13, plots of the irreversible energy rate Φ_{ir} for both thin and thick specimens are given versus the effective crack extension $\Delta\alpha_{\text{eff}}$. It is shown that again there is a crack propagation region where the energy increases and its length has nearly the same value as in Fig. 12. However, in that case the plateau values for thin and thick specimens appear more significantly different. This plateau value for the thin specimen was $\Phi_{ir}^{\text{thin}} = 0{\cdot}5$–$1\,\text{kJ m}^{-2}$ and for the thick specimen configuration was $\Phi_{ir}^{\text{thick}} = 1{\cdot}5$–$2\,\text{kJ m}^{-2}$. Figure 14 shows the crack resistance $R(= G_R^* + \Phi_{ir})$ versus the effective crack extension, $\Delta\alpha_{\text{eff}}$. The total plateau value for the thin specimen is about $R^{\text{thin}} = 4\,\text{kJ m}^{-2}$ while for the thick one $R^{\text{thick}} = 6\,\text{kJ m}^{-2}$.

Comparing these values to the ones calculated by the application of the monotonic tensile loading on CT samples and the compliance calibration technique, they are lower, and for the thick specimen there is a difference of 25%. This difference increases to 40% in the case of thin specimens.

There is a general consensus, based on the above results, that the monotonic tensile loading overestimates the fracture resistance of the material. Figure 15(a) shows a SEM micrograph of the fracture surface in the case of thick specimen under cyclic loading. Extensive pull-out which results in long pull-out length of about 1·5 mm, or even more, is easily recognized. In Fig. 15(b), a SEM micrograph of the lateral surface of pull-out fibers is presented, from which it is obvious that no matrix fragments remain on the fiber after pull-out.

Both Fig. 15(a) and (b) support the concept of prevalent transverse damage which is indicative of class III material. As has been proven in Ref. 15, the presence of a shear band in a notched tensile specimen redistributes the stresses ahead of the crack tip and the development of the shear damage

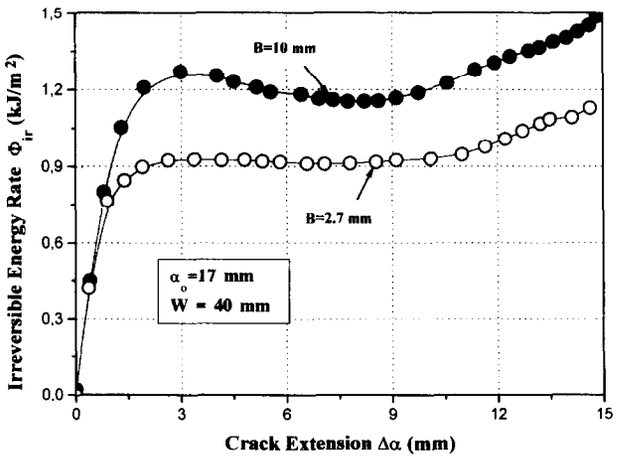

Fig. 13. Plastic energy dissipated rate, Φ_{ir}, versus effective crack extension, $\Delta\alpha_{\text{eff}}$, for thin ($B = 2{\cdot}7$ mm) and thick ($B = 10$ mm) specimens.

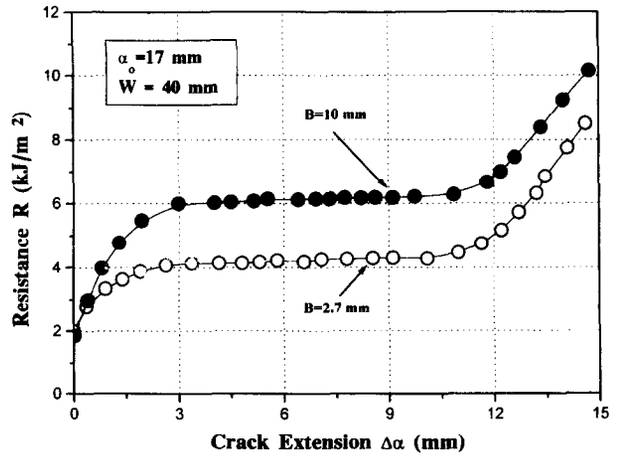

Fig. 14. Energy resistance, R, versus effective crack extension, $\Delta\alpha_{\text{eff}}$, for thin ($B = 2{\cdot}7$ mm) and thick ($B = 10$ mm) specimens.

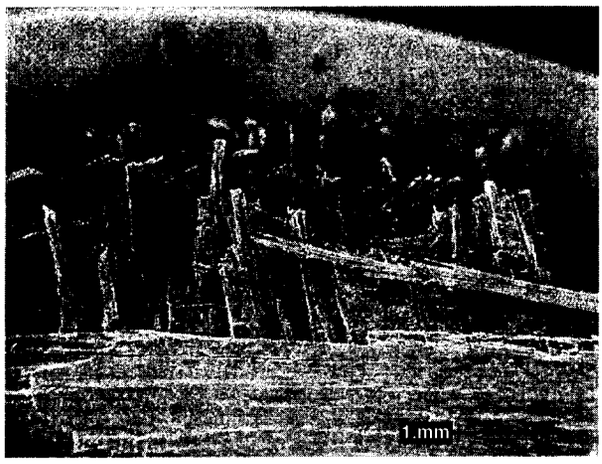

(a)

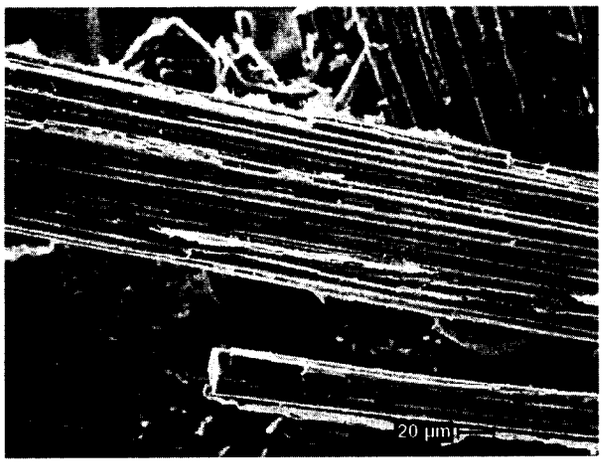

(b)

Fig. 15. SEM microphotographs, (a) fracture surface of thick specimen, pull-out length ~1·5 mm; (b) fractured fiber bundles.

reduces dramatically the stress within the range of $x/\alpha_o = 0{\cdot}1$.

Comparing the size of the stress redistribution zone mentioned above, to the size of the region where the fracture energy increases until the full development of the damage zone, it is concluded that they are almost identical. Nevertheless, the cyclic loading pattern for the characterization of the fracture behaviour of C/C composites seems to be the most appropriate, since it reveals completely the class III character of the material under investigation.

6 Conclusions

An effort has been made to evaluate the different testing techniques for the characterization of the fracture parameters of 2-D C/C composites through the evaluation of their R-curve behaviour. Based on the use of compact tension test geometry, monotonic tensile loading and cyclic loading have been applied to two different specimen thicknesses.

In all the cases a stress redistribution mechanism around the crack tip was detected, which mainly consisted of the formation of shear bands of narrow width which give rise to relatively large pull-out lengths. This is the typical class III material behaviour, as introduced in Ref. 15.

Furthermore, it was found that the loading–unloading testing procedure leads to a more realistic and consistent calculations, where the contribution of the crack tip phenomena and the stress shielding mechanisms, which enhance the material crack resistance to the material fracture behaviour, are calculated separately.

This approach appears to provide consistent prediction of the fracture resistance of the 2-D C/C composites. However, considerable additional data and, probably, a modification to CT geometry used (in order to secure a more extensive stable crack propagation zone) would be required for the assessment of the applied technique as a reliable methodology for the fracture characterization of the CMCs.

References

1. Lamicq, P. and Boury, D., Ceramic matrix composites parts design. AGARD-R-795. Introduction of ceramics into aerospace structural composites, 1993.
2. Schoberth, A. W., Condliffe, I., Michorious, M., Kostopoulos, V., Martin, E. and Anifrany, J. C., Development and characterization of CMC and C/C Composites. Report on BRITE/EURAM, Contract N. BREU 0334-C, 1994.
3. Krenkel, W., CMC Design consequences. Introduction of ceramics into aerospace structural composites, AGARD-R-795, 1993.
4. Evans, A. G., The mechanical properties of reinforced ceramics, metal and intermetallic matrix composites. *Materials Science and Engineering*, 1991, **63**, 63–76.
5. Evans, A. G. and Zok, F. W., The mechanical performance of ceramic matrix composites. *Journal of Materials Science*, 1994, **29**, 3857–3896.
6. Mackin, T. J., Perry, K. E., Epstein, J. S., Cady, C. and Evans, A. G., Strain fields and damage around notches in ceramic-matrix composites. *Journal of the American Ceramic Society*, 1996, **79**(1), 65.
7. Liorca, J. and Elices, M., Fracture resistance of fiber-reinforced ceramic matrix composites. *Acta Metallurgica et Materiallia*, 1990, **38**(12), 2485.
8. Rouby, D., Interface mechanisms in ceramic–ceramic fibre composites and their relation with fracture and fatigue behaviour. In *Proceedings of the 6th International Conference on Fracture Mechanics of Ceramics*, Stuttgart, 1995.
9. Cox, B. N., Extrincic factors in the mechanics of bridged cracks. *Acta Metallica Materials*, 1991, **38**(6), 1289.
10. Cox, B. N. and Marshall, D. B., Concepts for bridged cracks in fracture and fatigue. *Acta Metallica Materials*, 1994, **42**(2), 341.
11. Kostopoulos, V., Vellios, L., Christopoulos, G. C., Martin, E., Bouyou, S. and Lorriot, T., Fracture behaviour of 2-D carbon/carbon composites. In *Proceedings of the 8th CIMTEC*, Florence, 1994.
12. Bouquet, M., Birbis, J. M. and Quenisset, J. M., Toughness assessment of ceramic matrix composites. *Composite Science and Technology*, 1990, **37**, 223.

13. R'Mili, M., Rouby, D. and Fantozzi, G., Energy toughness parameters for a 2-D carbon fibre reinforced carbon composite. *Composite Science and Technology*, 1990, **37**, 207.
14. Cao, J. W. and Sakai, M., The crack face bridging of brittle matrix composites. In *Proceedings of the 6th International Conference on Fracture Mechanics of Ceramics*, Stuttgart, (1995).
15. Heredia, F. E., Spearing, S. M., Mackin, T. J., He, M. Y., Evans, A. G., Mosher, P. and Brondsted, P., Notch effect in carbon matrix composites. *Journal of the American Ceramic Society*, 1994, **77**(11), 2817–2827.
16. Begley, J. A. and Landes, J. D., The J integral as a fracture criterion, Part II. In ASTM STP No. 514, *Fracture Toughness*, Philadelphia, 1972, pp. 1–23.
17. Mai, Y. W. and Hakeem, M. I., Slow crack growth in cellulose fibre cements. *Journal of Material Science*, 1984, **19**, 501–511.
18. Kostopoulos, V. and Markopoulos, Y. P., On the fracture tougnhess of ceramic matrix composites. *Materials Science Engineering A*, (in press).